RSC Advances

PAPER

View Article Online
View Journal | View Issue

Cite this: *RSC Adv.*, 2024, **14**, 38302

Sensing behavior of CdS-TiO_2 thick films for the detection of hydrocarbons

Ankit Kumar Vishwakarma, *[a] Ajaya Kumar Sharma,[a] Arpit Verma,[b] B. C. Yadav[b] and Lallan Yadava[a]

In this article, the sensing behaviors of undoped titanium dioxide (TiO_2) and CdS-doped TiO_2 (CdS-TiO_2) thick films are discussed. Sensing pastes of 2 wt% CdS-TiO_2 and undoped TiO_2 were prepared in the laboratory and used to fabricate thick film gas sensors on an alumina substrate. The crystal structures of TiO_2 and CdS-TiO_2 samples were characterized by XRD and atomic force microscopy (AFM). The results indicated that the grain size and RMS roughness parameter were reduced by adding CdS contents. The sensing behaviors of the fabricated devices were studied at varying concentrations (0–5000 ppm) of different hydrocarbon gases, such as LPG, methanol, ethanol, toluene, and benzene, in ambient air at 300 K. The effect of humidity levels on the sensing properties of the sensors was also investigated. The sensor response value of CdS-TiO_2 for benzene was found to be 2.25 times higher than that of TiO_2-based sensing devices. Thus, CdS doping significantly enhanced the response and recovery times of the sensor. The TiO_2 film exhibited response and recovery times of 65 s and 180 s, respectively. In contrast, when doped with CdS, the response times were reduced to 15 s and 103 s, respectively, when exposed to benzene at a concentration of 5000 ppm at 300 K. The sensing mechanism has been discussed and the experimental results were validated using a model based on the Frenkel–Poole theory of electronic emission and catalytic oxidation. The obtained results demonstrate that TiO_2 structures doped with low concentrations of CdS exhibit superior sensitivity and selectivity to benzene gas under low humidity levels at room temperature (300 K).

Received 11th August 2024
Accepted 15th November 2024

DOI: 10.1039/d4ra05824k

rsc.li/rsc-advances

1. Introduction

In recent years, the necessity for the development of sensitive and stable hydrocarbon gas sensors has increased significantly. Detection of hydrocarbons and volatile organic compounds (VOCs), such as benzene, and toluene gases, is a subject of growing importance in domestic and industrial purposes. n-Type semiconductor oxides, such as TiO_2, SnO_2, ZnO, and WO_3, have been extensively investigated as chemo-resistive gas sensors.[1,2] Among these, TiO_2 is a promising material, which is frequently used in industry, research, and environmental monitoring. Due to its semiconducting nature and better chemical properties, several researchers have used TiO_2 and its dopants, such as Pd,[3] Pt,[4] Al,[5] Nb,[6] (Er^{+3}),[7] and Cr,[8] to detect a wide variety of gaseous species, including O_2,[9] H_2,[10] CO,[11] NO_x[12] LPG and benzene.[13] The combination of CdS and TiO_2 has been the most useful in detecting toxic, inflammable, and hazardous gases and is used in solar cells and photocatalytic applications.[14] A. L. Micheli developed the first TiO_2 gas sensor which was primarily used to detect stoichiometric air-to-fuel ratios.[15] According to a research by S. Shao *et al.*, hierarchical nanospheres made of rutile and anatase phases show superior gas sensing capacities at ambient temperature, in either an n-type or p-type fashion. The researchers found that the addition of Pt decorations had a significant impact on limiting the grain size, increasing the surface area, and regulating the particle size. Particularly, it was demonstrated that altering particle size and increasing surface area increased sensitivity to ethanol (an n-type property) and benzene (a p-type property), respectively, at ambient temperature.[16] Y. Wang *et al.* studied the synthesis and gas sensing properties of La and V co-doped TiO_2 thick films.[17] They observed that conductance increased with V and La doping and could inhibit the transformation from the anatase to rutile phase. The gas sensor based on La and V doping thick films showed excellent response to methylbenzene. D. Zhang *et al.* reported the fabrication of a Pd-decorated TiO_2/MoS_2 ternary nanocomposite for enhanced benzene gas sensing performance at room temperature, and they found that the fabricated sensor exhibited a high response, fast response–recovery time, repeatability, and good selectivity toward benzene.[18] H. Bian *et al.* investigated the characterization and gas-sensing properties of electrospun TiO_2 nanorods, concentrating on their acetone sensitivity. They found that while

[a]*Department of Physics, Deen Dayal Upadhyaya Gorakhpur University, Gorakhpur, U.P. 273009, India. E-mail: kv.ankit92@gmail.com; nisaly06@rediffmail.com*
[b]*Nanomaterials and Sensors Research Laboratory, Department of Physics, Babasaheb Bhimrao Ambedkar University, Lucknow-226025, U.P., India*

detecting acetone gas, these TiO_2 nanorods exhibited quick reaction times, maximum sensitivity, increased selectivity, and long-term stability. These results led the scientists to the conclusion that TiO_2 has a lot of potential as a material for the high-temperature detection of acetone.[19]

Benzene is widely used in chemical processes to produce products such as plastics, pesticides, pharmaceuticals, and other chemicals.[20] Benzene is a carcinogen having hazardous properties, which causes health issues, particularly in urban areas. Therefore, it is imperative to monitor benzene for health and safety. In the present research work, for the detection of benzene, a sensing device based on the CdS-TiO_2 structure has been investigated. The influence of CdS content on the microstructural properties and its sensing capability for various gases, including toluene, benzene, ethanol, methanol, and LPG, at room temperature have been investigated. The effect of humidity levels is also studied. A smaller CdS content (2 wt%) remarkably enhanced the sensitivity of TiO_2 to benzene gas in comparison to other test gases. The sensing mechanism and experimental results were justified by mechanistic and experimental results.

2. Experimental details

2.1. Fabrication of thick film sensor and sensing setup

Undoped TiO_2 (S_1) and 2 wt% CdS-doped TiO_2 (S_2) thick films having dimension of 8 mm × 8 mm were fabricated on alumina substrate of dimension 25 mm × 25 mm. The finger electrode pattern was printed using silver conductor paste (paste FD6176) on the front side, and the heater electrode pattern was printed using ruthenium oxide-based resistor paste (paste NTC 2413 ESL) on the backside of the substrate. The printed thick films were annealed at 250 °C for 90 min to ensure good adherence of the sensing layer on the substrate. For the measurement of the responses of the sensors (S_1, S_2) we designed a locally made glass chamber of volume 2047 mL in which provisions were made for the injection of gas and electrical connections. The electrical resistance of the sensors was measured with varying concentrations (0–5000 ppm) of different test gases, including benzene, toluene, methanol, ethanol, and LPG, at a temperature of 300 K using the experimental setup shown in Fig. 1.[21]

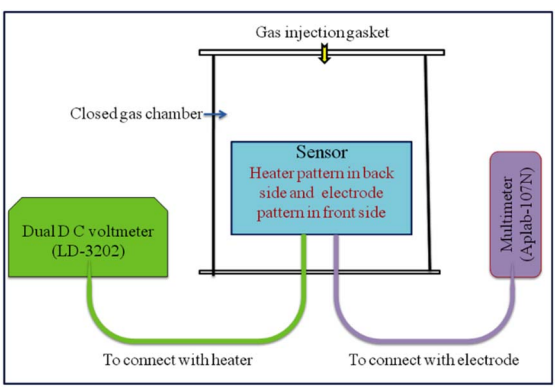

Fig. 1 Block diagram of the measurement setup.

2.2. Characterization

The microstructural properties of the fabricated thick film sensors S_1 and S_2 were studied using X-ray diffraction (XRD) and atomic force microscopy (AFM). XRD pattern was obtained by a D8-advanced equipped with Cu Kα_1 radiation of wavelength 0.15406 nm, while surface morphology was investigated using AFM. The AFM image was recorded with the digital instrument, Nanoscope-IV, with a Si_3N_4 100 μm cantilever and 0.58 N m^{-1} force constants in contact mode.

3. Results and discussion

3.1 Microstructural properties

The Scherrer formula[22,23] was used for the calculation of the average crystallinity of the fabricated samples:

$$D = \frac{K\lambda}{\beta \cos \theta} \quad (1)$$

where D is the average size of the crystallite, $K = 0.94$ Å, β = full-width half maxima (FWHM) of the diffraction peak and θ is the angle of diffraction. The XRD pattern shows a high-intensity peak centered at 25.7°, which is assigned to the TiO_2 plane (111). Other low-intensity peaks are assigned to the planes (211), (222), (200), (123), and (113). The XRD patterns of S_1 (undoped-TiO_2) and S_2 (2 wt% CdS-TiO_2) are shown in Fig. 2. The minimum crystallinities of TiO_2 and 2 wt% CdS-TiO_2 were 45.2 nm and 39.1 nm, respectively, with d spacing and FWHM of 1.775 Å and 0.1881°, respectively, indicating their nanocrystalline nature in the anatase phase. S. H. Mohamed *et al.*[14] studied the microstructural, optical, and photocatalytic properties of CdS-doped TiO_2 thin films. They prepared CdS doped TiO_2 thin films on glass substrates with higher CdS contents (3, 6, 9, and 12 wt%) and showed that there are 3.35% and 5.32% reductions in crystallite size at 3 wt% and 6 wt% CdS contents, respectively. However, larger reductions in crystallite size, ~13.49%, were found in the present investigation with smaller (2 wt%) CdS-

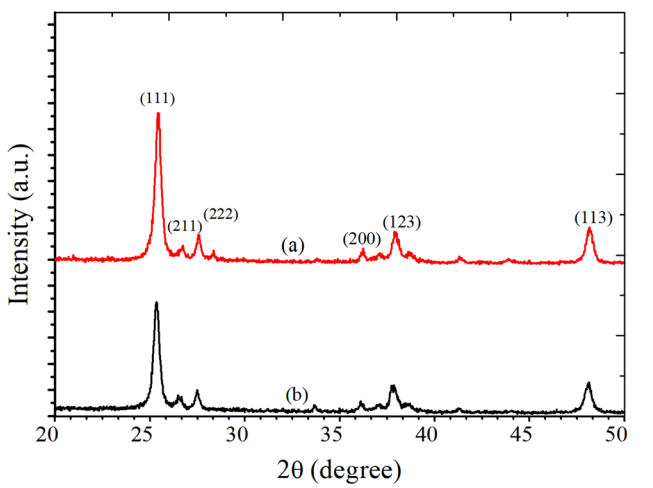

Fig. 2 XRD patterns of (a) S_1 and (b) S_2 sensors.

doping in TiO_2. The large reduction in the crystallite size played a vital role in enhancing the sensing response to test gases.

Earlier, Vishwakarma *et al.*[24] reported XANES (X-ray absorption near-edge spectroscopy) analysis and structural properties of CdS-doped TiO_2 films. The result demonstrated that CdS induced a modification in the electronic structure of TiO_2 film. It was observed that 2 wt% CdS-doping results in a phase change to the rutile phase from the anatase phase. The surface morphology of the deposited TiO_2 film for various concentrations of CdS was investigated using AFM at room temperature in the non-contact mode. The AFM signal was recorded over an area of 250 × 250 nm^2. The obtained data were plotted using the software WSxM.5.0 Develop.8.3. The surface morphology of the film strongly depended upon the CdS dopant concentration. The average grain size was obtained by statistically fitting the distribution curve with the Gaussian function, and it was found that the grain size reduced with CdS content (Fig. 4). The decrease in crystallite size of TiO_2 with CdS doping was consistent with XRD measurements and confirms that the fabricated structures are polycrystalline. AFM 3D and bar diagrams for sensors S_1 and S_2 are presented in Fig. 3(a–d). The crystallite size, grain size, roughness, rms roughness, and surface skewness are listed in Table 1. It is observed that the surface skewness of the samples increases with CdS concentration. It is evident from Fig. 3(c and d) that grain size and roughness are reduced with CdS-doping, as listed in Table 1. The reduction in crystallite size, grain size, and roughness with 2 wt% CdS contents leads to enhancing the sensing capability of the films for various gases, including benzene, methanol, ethanol, LPG, and toluene.

Table 1 Crystallite size, grain size, roughness, and skewness of S_1 and S_2 sensors

Sensor no.	Crystallite size (nm)	Grain size (nm)	Roughness (nm)	Surface skewness
S_1	~45.2	~63.2	~23.2	−0.331
S_2	~39.1	~52.4	~16.1	0.201

3.2. Gas sensing behavior and mechanism

The response of the sensor was determined using the following formula:

$$S = \left(\frac{R_a - R_g}{R_a}\right) \times 100 \quad (2)$$

where R_g and R_a are the resistance of the sensor in the presence of gas and clean air, respectively.[25,26] The response of sensors S_1 and S_2 against gas concentrations is demonstrated in Fig. 4(a–e). Fig. 4(a) represents the response of sensors S_1 and S_2 to benzene. It is evident from Fig. 4(a) that the response (63) of sensor S_2 is 2.25 times higher than that of sensor S_1. Fig. 4(b) delineated the response to methanol gas and it is 31 and 42, for sensors S_1 and S_2, respectively. The responses of sensors S_1 and S_2 to toluene, ethanol, and LPG, are presented in Fig. 4(c–e). The responses of sensor S_1 to toluene, ethanol, and LPG were 23, 23, and 10, while those of sensor S_2 to the same gases were 33, 28, and 15, respectively. Comparative sensor S_2 responses to different concentrations of ethanol, benzene, LPG, methanol, and toluene at room temperature are shown in Fig. 4(f). According to the ratio of maximal sensor S_2 responses, the response to benzene was the greatest, which was approximately

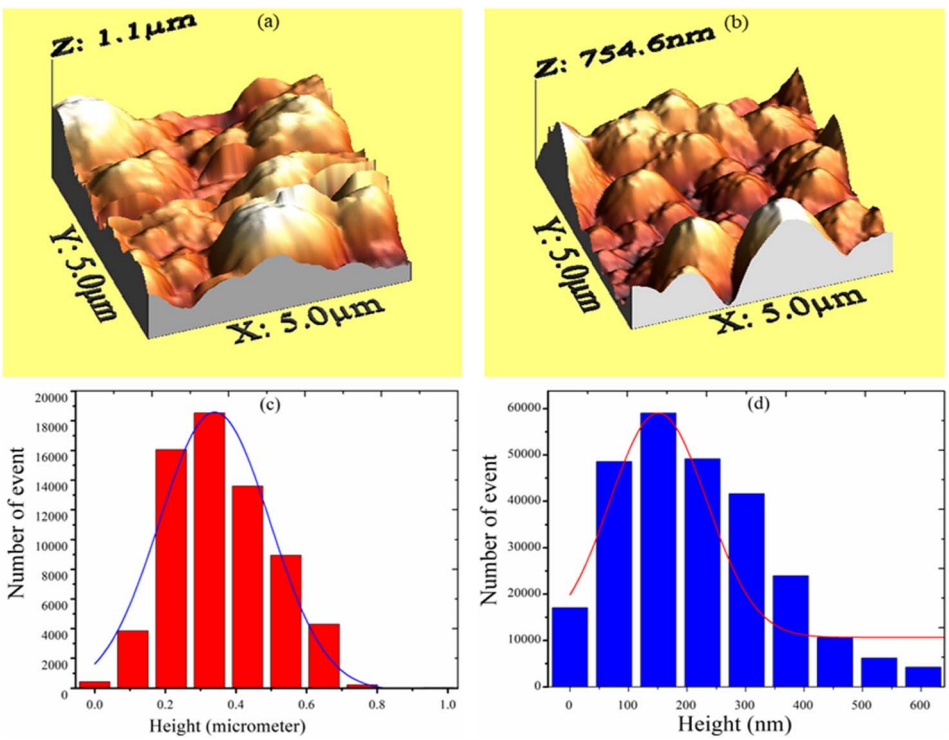

Fig. 3 AFM 3-D structure for sensor (a) S_1, (b) S_2 and AFM histogram of sensor (c) S_1, (d) S_2.

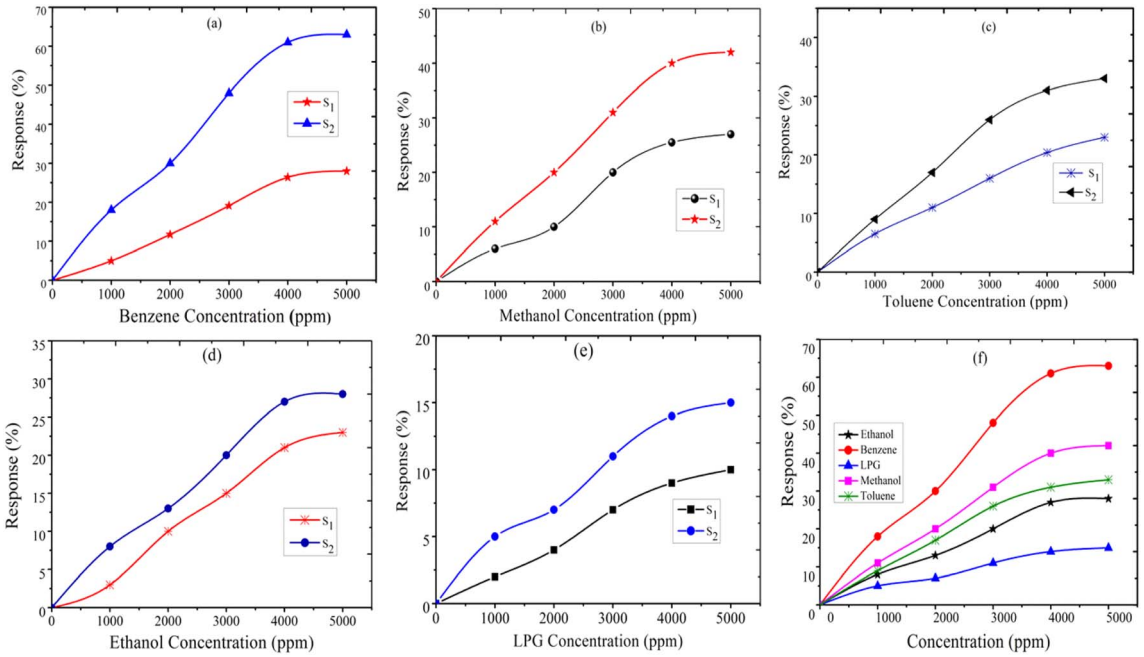

Fig. 4 The response of sensor S_1 and S_2 to (a) benzene, (b) methanol, (c) toluene, (d) ethanol, (e) LPG, and (f) comparative response of sensor S_2 to test gases.

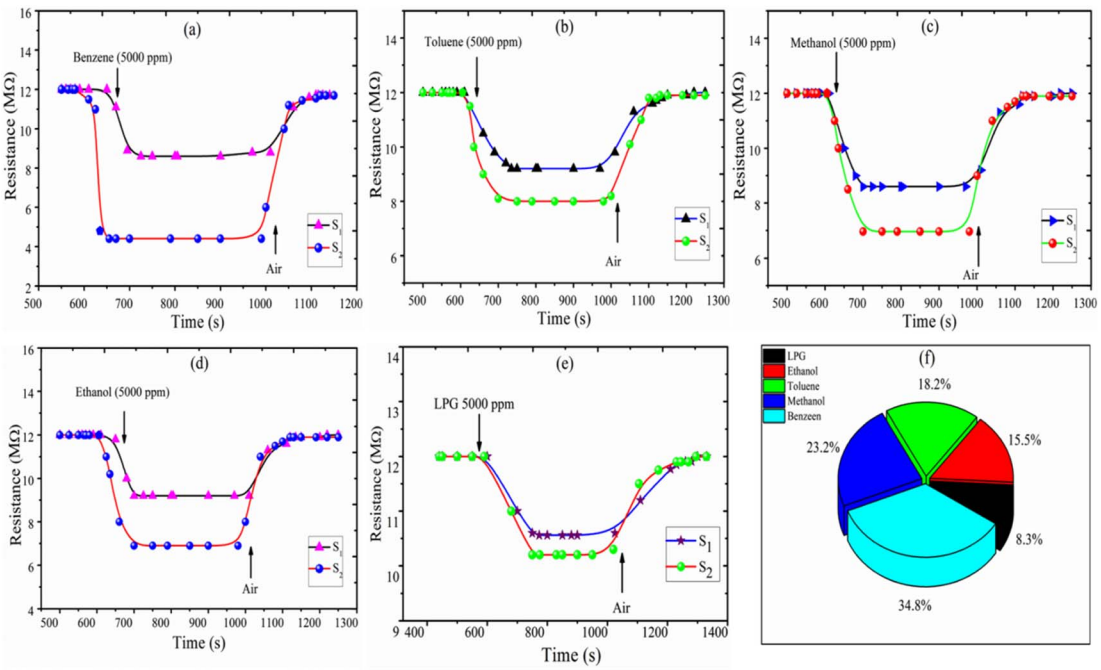

Fig. 5 Resistance of sensors S_1 and S_2 *versus* transient response time (s) for (a) benzene, (b) toluene, (c) methanol, (d) ethanol, (e) LPG, and (f) the selectivity of ethanol, LPG, methanol, toluene, and benzene for the S_2 sensor.

4.2 times higher than that of LPG, 2.25 times higher than that of ethanol, 1.5 times higher than that of methanol, and 1.92 times higher than that of toluene. As shown in Fig. 5(f), the sensor response measurements of S_1 and S_2 show that CdS doping leads to a significant improvement in the response and is more selective to benzene over other test gases.

Selectivity is one of the most important parameters of the sensor and is defined as:[21–27]

$$(\mathrm{Sel})_i = \frac{S_i}{\sum (S_i)} \times 100 \quad (3)$$

where S_i is the response to the test gas and $\Sigma(S_i)$ is the sum of the responses to all tested gases. Here, we calculated selectivity using eqn (4) as follows:

$$(\mathrm{Sel})_i = \left[\frac{S_i}{S_{\mathrm{toluene}} + S_{\mathrm{methanol}} + S_{\mathrm{LPG}} + S_{\mathrm{ethanol}} + S_{\mathrm{benzene}}}\right] \times 100 \quad (4)$$

The selectivity of sensors S_1 and S_2 for benzene, methanol, ethanol, LPG, and toluene gases are displayed through the Pi diagram, and it is ~34.8%, ~23.2%, ~15.5%, ~8.3%, and ~18.2%, respectively. It can be seen from Fig. 5(f) that sensor S_2 is more selective to benzene than to other test gases.

The resistance *vs.* transient response and recovery curve of the fabricated thick film sensors S_1 and S_2 at a 5000 ppm concentration of the benzene, toluene, methanol, ethanol, and LPG gases, are shown in Fig. 5(a–e). The response time is evaluated by the time taken to attain 90% of the maximum response with exposure to gases and the recovery time is measured as the time taken to reach 10% of the initial value in the absence of test gases. Fig. 5(a) shows that the response time and recovery time of sensor S_2 reduced from 65 s to 25 s and 180 s to 103 s, respectively, for benzene (5000 ppm at 300 K). The response and recovery time curves of toluene, methanol, ethanol, and LPG gases are plotted in Fig. 5(b–e). The comparative response, selectivity, response time, and recovery time of the sensors S_1 and S_2 for test gases are shown in Table 2. The measurement shows that the 2 wt% CdS doped TiO_2 thick film sensor S_2 is a suitable detector for benzene with better response and selectivity.

A theoretical model is presented to describe the sensing behavior of the fabricated CdS-TiO_2 thick film sensor (S_1 and S_2). A relation between response S and the concentration of gas C is given by.[28]

$$S = 1 - \exp(\mu_g \cdot F_p \cdot C^b) \quad (5)$$

where μ_g is an arbitrary constant (A^{-1} cm^2) whose value depends on the gas under consideration and the geometry of the sensing film, C is the gas-concentration in percentage (the ratio of vapor volume to chamber volume), b is a dimensionless constant, and F_P is the Frenkel–Poole emission constant.

$$\therefore S = \frac{R_a - R_g}{R_a} \text{ or } S = \left(1 - \frac{R_g}{R_a}\right)$$

Table 2 Response, selectivity, response time, and recovery time for thick film sensors S_1 and S_2

	Response (%)		Selectivity (%)	Response time (s)		Recovery time (s)	
Hydrocarbons	S_1	S_2	S_2	S_1	S_2	S_1	S_2
Benzene	**28**	**63**	**34.8**	**45**	**15**	**88**	**73**
Toluene	23	33	18.2	90	76	199	172
Methanol	27	42	23.2	89	72	200	155
Ethanol	23	28	15.5	96	85	199	181
LPG	10	15	8.3	95	83	210	181

Using eqn (2) and (5) we have,

$$\left(1 - \frac{R_g}{R_a}\right) = (1 - \exp(\mu_g \cdot F_p \cdot C^b))$$

$$\left(\frac{R_g}{R_a}\right) = (\exp(\mu_g \cdot F_p \cdot C^b)) \quad (6)$$

Taking the log of both sides of eqn (6)

$$\log\left(\frac{R_g}{R_a}\right) = ((\mu_g \cdot F_p \cdot C^b)) \quad (7)$$

Again, taking the log of both sides eqn (7) we have,

$$\log\left[\log\left(\frac{R_g}{R_a}\right)\right] = \log(\mu_g \cdot F_p \cdot C^b)$$

$$\therefore [\log(m \cdot n) = \log(m) + \log(n)]$$

$$\because \log\left[\log\left(\frac{R_g}{R_a}\right)\right] = \log(\mu_g \cdot F_p) + b \cdot (\log C) \quad (8)$$

Comparing eqn (8) with $Y = m \cdot X + A$.

Here slope $m = b$ (constant) and intercept $A = \log(\mu_g \cdot F_p)$.

Where F_p is the Frenkel–Poole emission constant and is defined as:

$$F_p \approx \varepsilon \exp\left[\frac{e\left(\sqrt{\frac{e\varepsilon}{\pi}}\right)}{kT} - \frac{e \cdot \phi_B}{kT}\right] (\mathrm{A\ cm^{-2}}) \quad (9)$$

where ε = combined electric field (V cm^{-1}), e = electronic charge, φ_B = barrier height, k = Boltzmann constant, and T = absolute temperature. We know that the relation between voltage and the electric field is, $\varepsilon = V/d$. Thus, eqn (9) can be written as:

$$F_p = \frac{V}{d} \exp\left[\frac{a(\sqrt{V})}{T} - \frac{e \cdot \phi_B}{kT}\right]$$

where $a = \sqrt{\frac{e^3}{\pi \cdot k^2 \varepsilon d}}$ and is a constant.[28]

The logarithmic sensing response as a function of all-test gas concentrations, log C, is plotted in Fig. 6(a–e) portraying a linear logarithmic response ($R^2 = 0.9767$) with benzene concentration. The Frenkel–Poole emission constant parameter is found as $\mu_g \cdot F_p \approx (-0.630 \pm 0.068)$ while the constant parameter $b = (0.242 \pm 0.019)$. From Fig. 6(a), it is observed that the response increases more linearly up to 4000 ppm and then tends to attain stagnation beyond a concentration of 5000 ppm. The obtained experimental results fit with the proposed model and log(C) variation with $\log(R_a - R_g/R_a)$, producing a straight line. The comparative logarithmic concentration for the S_2 sensor is shown in Fig. 6(f).

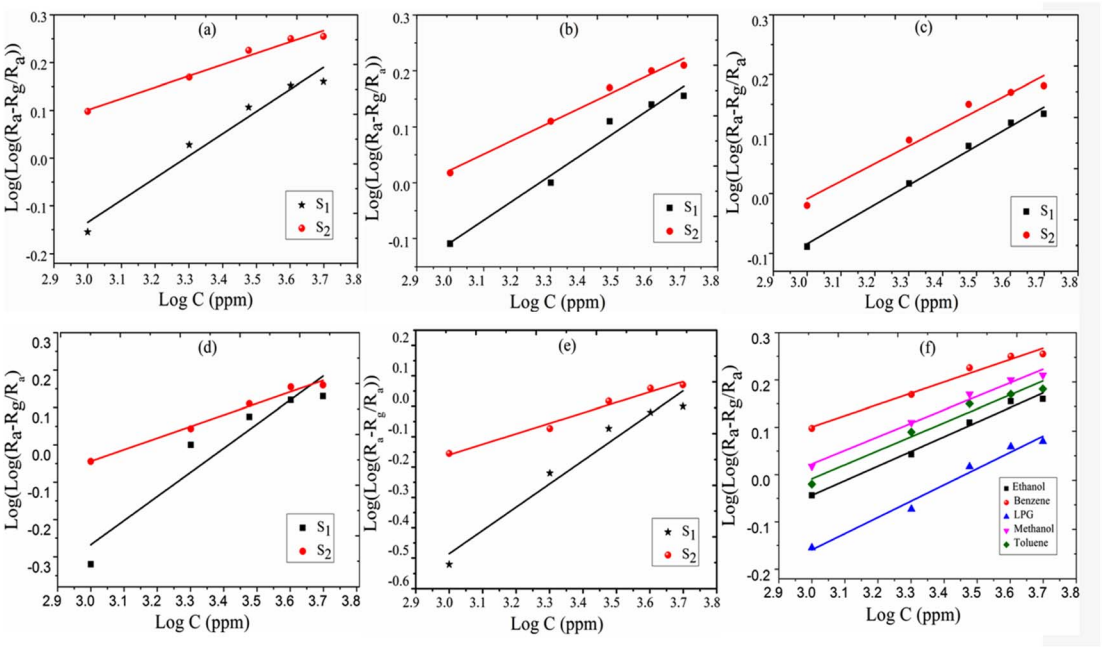

Fig. 6 Logarithmic presentation of sensing response *vs.* logarithmic presentation of test gas concentration (ppm) (a) benzene, (b) methanol, (c) toluene, (d) ethanol, (e) LPG; and (f) the comparative response for sensor S_2.

The response behavior of the fabricated sensors to the exposed hydrocarbon gases has also been explained based on adsorbed oxygen species and lower crystallite size of TiO_2 with CdS-doping. One of the important factors in controlling the response of a chemo-resistive metal oxide gas sensor is particle size (D).[29,30] Enhancement in the response of the fabricated sensor can be achieved through modulation of microstructural properties, specifically the grain size. Smaller grain sizes tend to yield superior gas sensing responses. However, it is crucial to strike a balance to ensure that the structural stability of the sensor is maintained. The response of a thick film sensor based on TiO_2 can be correlated with the characteristics of the space charge layer (L)[31,32] and it is reported that for $D < 2L$, the depletion layer does not restrict just at the surface but extends throughout the grain. The reduction in particle size with 2 wt% CdS-doping increases the alive surface area of the fabricated thick film sensor, which results in higher adsorption of oxygen species and increased response of sensors to the reducing gases.[33,34] A comparison table of sensing response, operating temperature, and response time for hydrocarbons is listed in Table 3.

When exceeding TiO_2 bandgap energy, the electron is promoted from the valence band to the conduction band TiO_2. The sensing mechanism of the fabricated sensors (S_1, S_2) can be determined as the resistance of materials varies with the oxygen molecules absorbed at the surface and the concentration of reducing gas species. When metal oxide comes in contact with air, oxygen molecules from the ambient air are adsorbed onto the surface of the metal oxide. At the grain boundaries electrons are trapped and a barrier is built around each grain. The adsorbed oxygen molecules are subsequently converted to ions after capturing an electron from the conduction band.[35] Eqn (10)–(13) are possible representations for the adsorption of the oxygen species (a, stands for air, ad stands for adsorption, and g stands for gas).[43,44]

$$O_{2(a)} \rightarrow O_{2(ads.)} \quad (10)$$

$$O_{2(a)} + e^- \rightarrow O_{2(ads.)}{}^- \quad (11)$$

$$O_{2(ads.)}{}^- + e^- \rightarrow 2O^- \quad (12)$$

$$2O^- + e^- \rightarrow O_{(ads.)}{}^{2-} \quad (13)$$

TiO_2 is an n-type semiconductor material with an electron as a majority carrier. When C_6H_6 molecules get in contact with the TiO_2 surface, adsorbed oxygen species readily interacts with hydrocarbons by releasing electrons back to the conduction band of TiO_2. Thereby, resistance decreases because of the electron-donating nature of C_6H_6 and subsequently the conductivity increases. The measurement reveals that the resistance of sensors S_1 and S_2 decreases with exposure to various test gases, namely, benzene, toluene, ethanol, methanol, and LPG in ambient air. The decrease in resistance of the sensor in the presence of benzene and other test gases may be due to decrease in the size of the depletion layer, as shown in the band diagram of CdS-TiO_2 thick film (Fig. 7). The understanding of the reaction mechanism on the CdS-TiO_2 surface in the presence of VOCs is represented as,

$$C_xH_y + nO^{m-} \rightarrow xCO_2 + H_2O + m \cdot ne^- \quad (14)$$

where m and n are integers. In the case of benzene $x = 6$, and if $m = 1$ or $m = 2$, then the possible reaction may be defined as eqn (15)–(19),

Table 3 Comparison table of sensing response, operating temperature, and response time for alcoholic and acetone gas

Sample	Text gas	Operating temperature (°C)	Sensitivity (%)	Response time (s)	References
CdS-TiO_2	Acetone	—	71	55	21
CdS-TiO_2	Propanol	—	63	62	27
CdS-SnO_2	Propanol	200	78	19	35
CdS-SnO_2	Toluene	200	51	—	36
PbO-SnO_2	Ethanol	200	88	—	37
Sb_2O_3-SnO_2	Ethanol	150	66	19	38
ZnO/TiO_2	Propanol	—	23	10	39
SnO_2 nanorods	Iso-propanol	325	11.2	6	40
SnO_2-Pd-Pt-In_2O_3	Methanol	160	320.7	32	41
Ce-doped SnO_2	Acetone	270	50.5	—	42
CdS-TiO_2	Benzene	27	63	15	Present work

$$C_6H_6 + 15O^- \rightarrow 6CO_2 + 3H_2O + 15e^- \quad (15)$$

Or

$$C_6H_6 + 15O^{2-} \rightarrow 6CO_2 + 3H_2O + 30e^- \quad (16)$$

Or

$$2C_6H_6 + 15O_2^- \rightarrow 12CO_2 + 6H_2O + 15e^- \quad (17)$$

Or

$$C_6H_6 + 12O^- \rightarrow 6CO_2 + 3H_2 + 12e^- \quad (18)$$

Or

$$C_6H_6 + 12O^{2-} \rightarrow 6CO_2 + 3H_2 + 24e^- \quad (19)$$

The possible reaction for ethanol is given in eqn (20)–(22)

$$C_2H_5OH + 6O^- \rightarrow 2CO_2 + 3H_2O + 6e^- \quad (20)$$

Or

$$C_2H_5OH + 6O^{2-} \rightarrow 2CO_2 + 3H_2O + 12e^- \quad (21)$$

Or

$$C_2H_5OH + 3O_2^- \rightarrow 2CO_2 + 3H_2O + 3e^- \quad (22)$$

The possible reaction for toluene is given in eqn (23) and (24)

$$C_6H_5OH + 14O^- \rightarrow 6CO_2 + 3H_2O + 14e^- \quad (23)$$

Or

$$C_6H_5OH + 14O^{2-} \rightarrow 6\ CO_2 + 3H_2O + 28e^- \quad (24)$$

The response of the fabricated sensors S_1 and S_2 towards benzene and other test hydrogen-containing gases can be explained based on eqn (14)–(24). When sensor S_2 is exposed to hydrogen-containing gases, such as benzene, toluene, methanol, ethanol, and LPG, the exposed gases react with oxygen anions present on the surface and may result from H atoms, some of which cross the interface of CdS/TiO_2. O. W. Johnson[45] already reported the diffusion of H_2 into TiO_2; these hydrogen atoms are ionized to produce conduction electrons and interstitial protons. During this reaction, some carriers may get trapped inside the TiO_2. Thus, it may be possible that there would be an increase in electrical conductivity with varying concentrations (0–5000 ppm) due to the high polarizability of TiO_2 lattice and increase in trap charges at the CdS/TiO_2 interface upon exposure to benzene. The faster response and recovery time of the sensor S_2 to the test gases is attributed to a change in barrier height at grain boundaries, which is due to

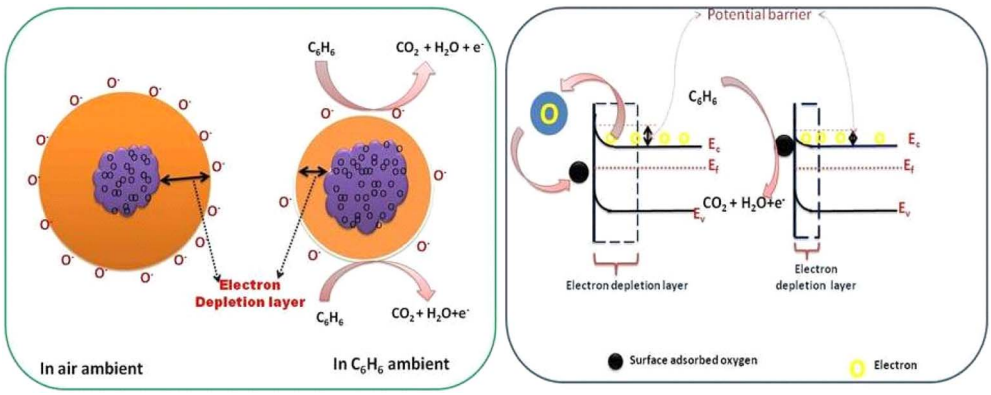

Fig. 7 Role of oxygen species and effect of CdS on the TiO_2 band structure for benzene gas detection.

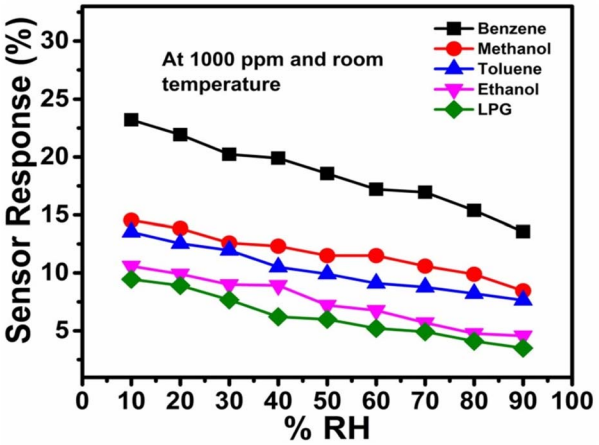

Fig. 8 Sensor responses to various analytes at different relative humidity levels.

exposure of test gases and their interaction on the surface of TiO_2–CdS, modulating the surface charge densities, which depend on temperature and gas exposure. Future work can be done regarding oxidation of target gases at room temperature in dry and wet conditions and its reaction with chemisorbed oxygen species.

3.3. Effect of relative humidity on sensing properties

The effect of relative humidity on gas sensor performance is a crucial aspect for sensor development, especially when aiming for operability at room temperature. Understanding how humidity levels affect gas response properties can lead to more accurate and reliable sensors. The performance of a CdS-TiO_2 chemo-resistive sensor at various relative humidity (RH) values for various gases is shown in detail in Fig. 8. It is clear from a detailed examination of Fig. 8 that for the majority of the studied gases, the effect of RH on sensor performance is constant; greater humidity levels are detrimental to sensor reliability in detecting the target gases. It is important to note that humidity levels at the higher end of the spectrum, between 70% and 90% RH, have the most significant impacts on the sensor response. Comparing the responses of the sensor to other gases under the same RH conditions, interesting patterns emerge. For instance, the sensor has the best response to benzene (23.21%) and the worst response to LPG (9.45%) at 10% RH. This shows that the sensor is most sensitive to benzene and least sensitive to LPG at low humidity levels. When using this sensor for applications that demand selective gas detection, these differences in sensitivity should be considered. The data also suggest RH levels at which there are considerable declines in sensor responsiveness. The sensor response to methanol, for instance, is 12.59% at 30% RH and 12.31% at 40% RH. This indicates that the sensitivity of the sensor towards methanol noticeably decreases between 30% and 40% RH. Finding these thresholds is essential for improving the performance of sensors in real-world situations with changing humidity levels. This sensor has some humidity sensitivity in terms of its anti-humidity capabilities. Despite changes in humidity levels, the ideal anti-humidity sensor would continue to respond consistently. However, this information shows that when RH rises, the performance of the sensor tends to deteriorate. Because of this, it might not be the ideal option for applications in high-humidity situations without extra moisture mitigation methods.

4. Conclusions

Under ambient room temperature conditions, the detecting capacities of two thick film sensors, S_1 (undoped) and S_2 (containing 2 wt% CdS-TiO_2), were investigated. The test gases included benzene, toluene, methanol, ethanol, and LPG. The sample with 2 wt% CdS combined with TiO_2 (S_2) had the most notable response, with a sensitivity of 63% for benzene gas. Measurements reveal that the sensor is more selective to benzene than to the other test gases; its selectivity lies at 34.8%, which is much higher than that of others (table). The higher response to exposure to benzene is due to a decrease in crystallinity with the increase in CdS contents and surface modifications of the CdS/TiO_2 structure. The addition of 2 wt% CdS in the TiO_2 sample was found to be effective in promoting the response and selectivity. Thus, we conclude that 2 wt% CdS-TiO_2 samples are good candidates for the growth of low-cost high-performance benzene (C_6H_6) gas sensors at room temperature and low humidity levels.

Data availability

Data are available on request.

Conflicts of interest

There are no conflicts to declare.

Acknowledgements

The authors are thankful to UGC-DAE Consortium for Scientific Research Indore for providing XRD and AFM measurements.

References

1 B. C. Yadav, R. Srivastava, C. D. Dwivedi and P. Pramanik, *Sensor. Actuator. B Chem.*, 2008, **131**, 216–222.
2 A. K. Vishwakarma and L. Yadava, *Environ. Sci. Pollut. Res.*, 2021, **28**, 3920–3927.
3 H. Kobayashi, K. Kishimoto, Y. Nakato and H. Tsubomura, *Sensor. Actuator. B Chem.*, 1993, **13**, 125–127.
4 L. A. Patil, D. N. Suryawanshi, I. G. Pathan and D. G. Patil, Nanocrystalline Pt-doped TiO_2 thin films prepared by spray pyrolysis for hydrogen gas detection, *Bull. Mater. Sci.*, 2014, **37**, 425–432.
5 F. Bayata, B. Saruhan-Brings and M. Urgen, Hydrogen gas sensor of nano-porous, *Sensor. Actuator. B Chem.*, 2014, **204**, 109–118.
6 S. K. Gautam, N. Gautam, R. G. Singh, S. Ojha, D. K. Shukla and F. Singh, Anomalous behavior of B_{1g} mode in highly

transparent anatase nano-crystalline Nb-doped titanium dioxide (NTO) thin films, *AIP Adv.*, 2015, **5**, 127212.
7 J. A. Barrego Perez, M. Courel, R. C. Valderrama, I. Hernandez, M. Pal, F. P. Delagado and N. R. Mathews, Structural, optical and photoluminces properties of erbium-doped TiO_2, *Vacuum*, 2019, **169**, 108873.
8 F. Bensouici, T. Souier, A. A. Dakhel, A. Iratni and M. Bououdina, Synthesis, characterization and photocatalytic behavior of Ag-doped TiO thin film, *Superlattices Microstruct.*, 2015, **85**, 255–265.
9 U. Kirner, K. D. Schierbaum, W. Göpel, B. Leibold and W. F. Chu, Low and high-temperature TiO_2 oxygen sensors, *Sensor. Actuator. B Chem.*, 1990, **1**, 103–107.
10 L. D. Birkefeld, A. M. Azad and S. A. Akbar, Carbon Monoxide and Hydrogen Detection by Anatase Modification of Titanium Dioxide, *J. Am. Ceram. Soc.*, 1992, **75**, 2964.
11 N. Bonini, M. C. Carotta, A. Chiorino, V. Guidi and M. Sacerdoti, oping of a nanostructured titania thick film: structural and electrical investigations, *Sensor. Actuator. B Chem.*, 2000, **68**, 274–280.
12 V. Guidi, M. C. Carotta, M. Ferroni, G. Martinelli and G. Sberveglieri, Preparation of nanosized titania thick and thin films as gas sensors, *Sensor. Actuator. B Chem.*, 1999, **57**, 197–200.
13 M. Mabrook and P. Hawkins, A rapidly-responding sensor for benzene, methanol, and ethanol vapor based on the film of titanium dioxide, *Sensor. Actuator. B Chem.*, 2001, **75**, 197–202.
14 S. H. Mohamed and E. R. Shaaban, Microstructural, optical and photocatalytic properties of CdS doped TiO_2 thin films, *Physica B*, 2011, **406**, 4327–4331.
15 A. L. Michaeli, *Am. Ceram. Soc. Bull.*, 1984, **63**, 694.
16 S. Shao, S. Wang, F. Jiang, H. Wu, T. Wu, Y. Lei, J. Fei and R. Koehn, Fabrication of anatase/rutile hierarchical nanospheres with enhanced n/p type gas sensing performance at room temperature, *R. Soc. Chem. Adv.*, 2016, **6**, 57722–57726.
17 Y. Wang and Y. Dai, Synthesis, and gas sensing properties of La and V co-doped TiO_2 thick films, *Funct. Mater. Lett.*, 2018, **11**(4), 1850019.
18 D. Zhang, C. Jiang and X. Zhao, Fabrication of Pd-decorated TiO_2/MoS_2 ternary nanocomposite for enhanced benzene gas sensing performance at room temperature, *Talanta*, 2018, **182**, 324–332.
19 H. Bian, S. Ma, A. Sun, X. Xu, G. Yang, J. Gao, Z. Zhang and H. Zhu, Characterization and acetone gas sensing properties of electrospun TiO_2 nanorods, *Superlattices Microstruct.*, 2015, **81**, 107–113.
20 V. S. Vaishnav, S. G. Patel and J. N. Panchal, Development of ITO thin film sensor for detection of benzene, *Sensor. Actuator. B Chem.*, 2015, **206**, 381–388.
21 A. K. Vishwakarma, A. K. Sharma, N. K. Yadav and L. Yadav, Development of CdS-doped TiO_2 nanocomposite as acetone gas sensor, *Vacuum*, 2021, **191**, 110363.
22 A. K. Vishwakarma and L. Yadava, fabrication and characterization of CdS doped ZnO nano thick film, *Vacuum*, 2018, **155**, 214–218.
23 A. K. Sharma, A. K. Vishwakarma and L. Yadava, *Mater. Lett.:X*, 2023, **17**, 100180.
24 A. K. Vishwakarma, S. S. Majid and L. Yadava, XANES analysis and structural properties of CdS-doped TiO_2, *Vacuum*, 2019, **165**, 239–245.
25 L. Yadava, R. Verma and R. Dwivedi, Sensing properties of CdS doped tin oxide thick film gas sensor, *Sensor. Actuator. B Chem.*, 2010, **144**, 37–42.
26 A. K. Vishwakarma, A. K. Sharma, A. K. Mishra and L. Yadava, *Mater. Lett.:X*, 2023, **17**, 100184.
27 A. K. Vishwakarma and L. Yadava, Detection of propanol gas using titanium dioxide-based thick film, *IOP Conf. Ser.:Mater. Sci. Eng.*, 2018, **404**, 012020.
28 L. Yadava, R. Verma and R. S. Singh, Detection and sensing mechanism with modeling using $Pd/TiO_2/Si$ structure, *Thin Solid Films*, 2013, **520**, 3039–3042.
29 Y. Shimizu and M. Egashira, Basic aspects and challenges of semiconductor gas sensors, *MRS Bull.*, 1999, **24**, 18–24.
30 S. Seal and S. Shukla, Nanocrystalline SnO_2 gas sensors given surface reactions and modifications, *J. Miner. Met. Mater. Soc.*, 2002, **54**, 35–38.
31 B. Rahmani, K. Yasouka and S. Ishii, Interaction of pulsed metal vapor plasma with insulator wall, *J. Appl. Phys.*, 2004, **95**, 11.
32 J. K. Srivastava, P. Pandey, V. N. Mishra and R. Dwivedi, Structural and microstructural studies of PbO-doped SnO2 sensor for detection of methanol, propanol, and acetone, *J. Nat. Gas Chem.*, 2011, **20**, 179–183.
33 D. M. Griffiths and C. H. Rochester, *J. Chem. Soc., Faraday Trans.*, 1994, **174**, 213.
34 M. El.-Maazawi, A. N. Finken, A. B. Nair and V. H. Grassian, Adsorption and photocatalytic oxidation of acetone on TiO_2: An in-Situ Transmission FT-IR Study, *J. Catal.*, 2000, **191**, 138–146.
35 A. K. Vishwakarma, A. K. Sharma and L. Yadav, *RSC Adv.*, 2024, **14**, 16459–16465.
36 P. Yadav, A. K. Sharma, S. K. Yadav, A. K. Vishwakarma and L. Yadava, *Mater. Today Proc.*, 2021, **38**, 2792–2796.
37 A. K. Vishwakarma and L. Yadav, Influence of PbO on SnO_2 thick film for sensing properties of toxic gas, *Appl. Phys. A*, 2024, **130**, 765.
38 P. Yadav, S. K. Yadav, A. K. Vishwakarma, D. S. Saini and L. Yadava, *Appl. Phys. A*, 2024, **130**, 119.
39 I. Gaidan, D. Brabozon and I. U. Ahad, *Sensors*, 2009, **17**(9), 1995.
40 D. Hu, B. Q. Han, R. Han, S. J. Deng, Y. Wang, Q. Li and Y. D. Wang, *New J. Chem.*, 2014, **38**, 2443–2450.
41 Y. X. Li, D. D. Deng, X. X. Xing, N. Chen, L. Xu, X. C. Xiao and Y. D. Wang, *Sens. Actuators, B*, 2016, **237**, 133–141.
42 X. Lian, Y. Li, X. Tong, Y. Zou, X. Liu and D. An, *Appl. Surf. Sci.*, 2017, **407**, 447–455.
43 A. Dey, Semiconductor-metal oxide gas sensor: Review, *Mater. Sci. Eng. B*, 2018, **229**, 206–217.
44 L. R. Skubal, N. K. Meshkov and M. C. Vogt, detection and identified of gaseous organics using a TiO_2 sensor, *J. Photochem. Photobiol., A*, 2002, **148**, 103–108.
45 O. W. Johnson, S. H. Pack and J. W. Deford, Diffusion of H and D in TiO_2: Suppression of internal fields by isotope exchange, *J. Appl. Phys.*, 1975, **46**, 1026.